AIAA Propulsion and Energy Forum
July 28-30, 2014, Cleveland, OH
50th AIAA/ASME/SAE/ASEE Joint Propulsion Conference

10.2514/6.2014-4027

Quasi-one-dimensional code for particle-in-cell simulation of magnetic nozzle expansion

Frans H. Ebersohn,* J.P. Sheehan,† Benjamin W. Longmier,‡
University of Michigan, Ann Arbor, MI, 48109, USA

John V. Shebalin§
Exploration Integration and Science Directorate, NASA Johnson Space Center, Houston, Texas, 77058

The formulation and validation of a novel quasi-one-dimensional particle-in-cell code for the simulation of magnetic nozzles is presented. Quasi-one-dimensional effects are included through virtual displacements of magnetized particles from the axis of symmetry and cross-sectional area variation according to preservation of magnetic flux. A modified, semi-implicit Boris algorithm is developed for capturing the Lorentz force effects in quasi-1D. Validation problems are selected to test the components of the code required to model the important physics of magnetic nozzles. Simulations are performed of two stream instabilities, Landau damping, source and collector sheaths, and magnetic mirrors. Results from the validation simulations show that the code produces physically accurate results when compared with both theory and other simulations.

Nomenclature

ρ	Charge Density	n	Number Density
T	Temperature	p	Pressure
v	Velocity	m	Mass
A	Cross Sectional Area	J	Current Density
B	Magnetic field	E	Electric Field
λ	Mean Free Path	L	Characteristic Length
ω	Frequency	τ_{col}	Collision Time
q	Charge of Electron	ν	Collision Frequency
Subscript			
$\perp$	Perpendicular to Magnetic Field	$\parallel$	Parallel to Magnetic Field
0	Initial	i	Ion
e	Electron	th	Thermal
p	Plasma	s	Species
c	Cyclotron	L	Larmor

I. Introduction

Electrodeless plasma thrusters are currently under development due to the potential advantages these thrusters present over other electric propulsion devices.[1–7] By limiting contact of plasma with surfaces, electrodeless thrusters can achieve longer lifetime and operate at more energetic, higher temperature conditions. A key component to many of the current electrodeless thruster designs is a guiding magnetic field which

*Graduate Student Researcher, Aerospace Engineering.
†Research Fellow, Aerospace Engineering.
‡Assistant Professor, Aerospace Engineering, AIAA Member.
§Senior Member

both controls the flow of the plasma and generates thrust. This magnetic field is known as a magnetic nozzle and is shown in Figure 1. This figure compares a de Laval nozzle and a magnetic nozzle. De Laval nozzles guide and accelerate a high temperature fluid generated in the combustion chamber to supersonic speeds by using a physical wall. Similarly, magnetic nozzles accelerate a high temperature plasma generated in the plasma source by using a strong guiding magnetic field.[8–10] Magnetic nozzles also have applications to improve performance of magnetoplasmadynamic thrusters.[11,12]

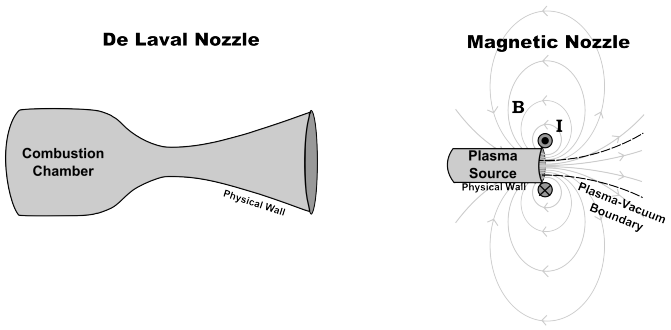

Figure 1: Comparison between de Laval nozzle and magnetic nozzle.

Key phenomena in the thrust generation process in magnetic nozzles are: i) the energy exchange between different modes leading to directed kinetic energy, ii) the transfer of momentum between the plasma and the magnets, and iii) the eventual detachment of the plasma from the closed magnetic field lines. The energy exchange behavior is of particular interest because it defines the physical mechanism by which axial kinetic energy is extracted from the plasma. Two of the mechanisms currently considered for this include thermal, electron-driven expansion[1,2,9,13–15] and the magnetic dipole force.[16–18]

Thermal, electron-driven acceleration of the ions occurs because the high temperature, low mass electrons expand into vacuum much more quickly than the massive, low temperature ions. Rapid electron thermal expansion generates an electric field which then accelerates the ions in order to maintain quasineutrality. By this mechanism the thermal energy of the electrons can be converted into directed kinetic energy of the ions. Experiments have shown that the potential structure which develops has characteristics of either a double layer or an ambipolar field.[4,13] The energy distribution and thermal behavior of the plasma during this expansion remains an open question.

The magnetic dipole force is the force that a magnetic dipole feels in the presence of an externally applied magnetic field.[19] This force is written as:

$$\mathbf{F}_d = \nabla(\boldsymbol{\mu} \cdot \mathbf{B}) \tag{1}$$

In this equation $\boldsymbol{\mu}$ is the vector magnetic dipole moment and $\mathbf{B}$ is the magnetic field. Particles in sufficiently strong magnetic fields behave like small magnetic dipoles and are described as being magnetized. The criteria for magnetization is satisfied when the Larmor radius of the particle, $r_L = mv_\perp/qB$, is much smaller than a characteristic dimension of the system. This length is typically defined as the gradient length scale which leads to the condition below.

$$\frac{r_L|\nabla B|}{|B|} \ll 1 \tag{2}$$

Furthermore, the collisionality of the species has to be low as defined by the Hall parameter written as:

$$\frac{qB}{m\nu} = \frac{\omega_c}{\nu} \gg 1 \tag{3}$$

This ratio compares the cyclotron frequency, ω_c, of the particle to the collision frequency, ν.

Diamagnetic particles always generate magnetic moments which are anti-parallel to the magnetic field. The magnetic moment for a magnetized particle is often assumed to be constant to simplify analysis, although it is not done so in our code. We present this simplification for illustrative purposes to give basic insight on

the physics, but do not make this assumption in our actual calculations in order to capture a more general solution. This leads to a more simplified form of the equation shown in Equation 4.

$$\mathbf{F}_d = -\mu \nabla \mathbf{B} \tag{4}$$

Equation 4 shows how this force repels a particle which is moving into a region of strong magnetic field. One of the most common examples of the effects of this force are seen in devices known as magnetic mirrors.[20] In a magnetic mirror particles moving from a weak to a strong field region exchange kinetic energy from the modes along the field line to those perpendicular to the field line. This leads to confinement of some of the particles and a loss of others. In the expansion region of a magnetic nozzle (an inverted magnetic mirror) the opposite of this occurs as the perpendicular kinetic energy of the particle is converted to parallel kinetic energy. The dipole force is the mechanism by which the particle experiences acceleration and deceleration along the magnetic field line. The effects of this force have been previously studied mostly from an analytical perspective.[16,17]

Herein we present the formulation and validation of a quasi-one-dimensional particle-in-cell (PIC) code for studying plasma behavior in a magnetic nozzle which focuses on studying thermal, electron-driven expansion and dipole force energy exchange mechanisms from a kinetic perspective. The purpose of this code is to further investigate the conditions which lead to the development of ambipolar and double layer potential structures, expanding on previous work in this area.[7,13,15,21–23] This code will also be used to study the thermal behavior of the plasma and evolution of the velocity distribution function throughout the expansion. Mechanisms which affect the evolution of the velocity distribution of the particles such as collisions and instabilities will specifically be investigated. The code will capture the effects of both the electric and magnetic forces on the energy exchange process and the coupling between these mechanisms.

Section II describes the methodology for the quasi-one-dimensional magnetic nozzle PIC code and Section III presents validation test cases. Section IV concludes the paper and discusses future work.

II. Methodology

Particle-in-cell codes treat the constituent species of a plasma as particles.[24,25] These particles propagate in a domain which is divided into a grid of cells as shown in Figure 2. For the model presented in this paper a one dimensional grid is used and a two dimensional grid is shown here for illustrative purposes only. A flow chart for the code is also shown which will be described in greater detail below.

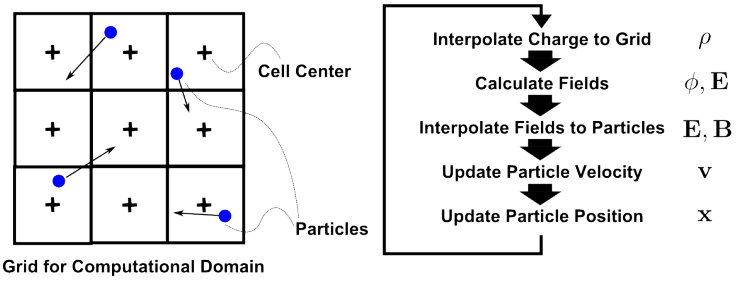

Figure 2: Particle-in-cell domain and flowchart.

First, the charge density for a cell is found by weighting the charge of nearby particles to the cell and then dividing by the cell volume. The charge density is collected at the cell centers and then used to solve Poisson's equation, Equation 5, for the potential.

$$\nabla^2 \phi = -\frac{\rho}{\epsilon_0} \tag{5}$$

In this equation ϕ and ρ are the potential and charge density respectively. Solving Poisson's equation gives the potential at the cell centers which is then used to find the electric field according to $\mathbf{E} = -\nabla\phi$. The electric field can be calculated at the cell centers or cell walls and is then weighted to the nearby particles. In the case of an electrostatic solver, the magnetic field is assumed to be constant and is also specified at the cell centers and then weighted to the nearby particles.

The weighted electric and magnetic fields are used with the equations of motion for the particles to change the position and velocity of the particles. The equations of motion are the change in position of the particles, $d\mathbf{x}/dt = \mathbf{v}$ and the change in velocity which is governed by the Lorentz force shown in Equation 6.

$$F = m\frac{d\mathbf{v}}{dt} = q(\mathbf{E} + \mathbf{v} \times \mathbf{B}) \tag{6}$$

Boundary conditions are applied at the edge of the domain and this process is repeated for the entire simulation. Typically, all of the particles in simulations of real world systems can not be resolved due to the high densities of particles and the limitations of computing power. This results in the use of macro-particles which represent a large number of particles instead of individual particles.

A. Quasi-1D Formulation

In this section we present the formulation for the electrostatic, quasi-one-dimensional (Q1D) PIC code developed for simulating magnetic nozzles. This solver resolves a single spatial dimension and three velocity dimensions, abbreviated as 1D3V. The spatial dimension resolved is the axis of symmetry of the magnetic nozzle, $\hat{z}$, shown in Figure 3. The grid is comprised of cell walls and cell centers at which different flow and field parameters can be located.

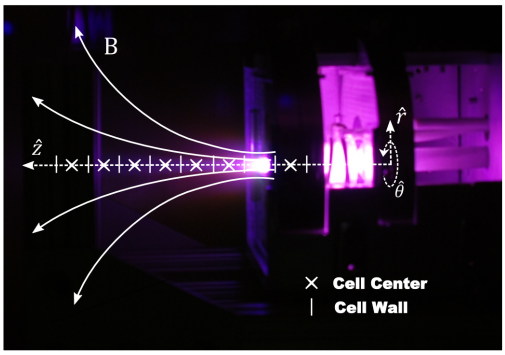

Figure 3: Quasi-1D domain superimposed on Cubesat Ambipolar Thruster magnetic nozzle experiment.

In Figure 3 the one dimensional domain is shown over the plume of the Cubesat Ambipolar Thruster(CAT). This propulsion device is currently being developed at the Plasmadynamics and Electric Propulsion Lab (PEPL) at the University of Michigan and is planned to be used as a propulsion system for nanosatellites.

1. *Virtual Larmor Radius Displacements*

On the axis of symmetry of the magnetic nozzle there is only an axial field, which implies that there will be no force due to the magnetic field in the axial direction. Therefore, the magnetic dipole force could not be captured in a strictly 1D model. This motivated the development of a novel Q1D method to include this force. First, we assume that all magnetized particles are virtually displaced from the axis of symmetry by their Larmor radius. To find the radial magnetic field we use the Gauss Law of Magnetism, $\nabla \cdot \mathbf{B} = 0$, expressed in cylindrical coordinates for an axisymmetric configuration in Equation 7.

$$\frac{1}{r}\frac{\partial}{\partial r}(rB_r) + \frac{\partial B_z}{\partial z} = 0 \tag{7}$$

The axial magnetic field is known from the initial conditions and we use this to calculate the radial magnetic field. Equation 7 is simplified by integrating over the radius and then using the virtual Larmor radius displacement of the particle as the radius. The result is shown in Equation 8 and holds as long as $\partial B_z/\partial z$ is approximately constant over r_L.

$$B_r = -\frac{r_L}{2}\frac{\partial B_z}{\partial z} \tag{8}$$

Equation 8 gives the approximate radial magnetic field a particle orbiting around the axis of symmetry would experience and can be used in the conventional particle pushing algorithms.

2. Cross-Sectional Area Variation

This model is further made quasi-one-dimensional by partially accounting for the expansion the jet undergoes. To do so we first assume that near the axis the particles approximately follow the magnetic field lines. This implies that the the cross-sectional area of the plasma jet is correlated to expansion of the magnetic flux tubes. By using Gauss Law of Magnetism in integral form, $\oint \mathbf{B} \cdot d\mathbf{S} = 0$, for a cylindrical, axisymmetric coordinate system and assuming that the contribution of the radial magnetic field flux is negligible we find a relation between the axial magnetic field and the cross sectional area. This relation is shown in Equation 9 which relates the inlet values of B_z and the cross-sectional area, A, to the cross-sectional area at a known axial magnetic field strength.

$$A = \frac{B_{z,in}}{B_z} A_{in} \tag{9}$$

It is important to note that the area now represents both the flux tube size and the cross sectional-area of the plasma jet. The variation of the cross sectional area has implications only on solving Poisson's equation and includes 2D effects due to the expansion of the plasma.

B. Algorithms Incorporated

Charges are interpolated and weighted to the cell using linear interpolation, also called cloud-in-cell interpolation.[24,25] Poisson's equation is solved by using the linear algebra package of the Intel Math Kernel Library. The electric fields are calculated at the cell boundaries from the potential by central differencing. For validation cases which are strictly 1D the Boris Particle Push is used.[26] The Boris push was modified for the Q1D cases due to axisymmetry and is described in more detail below. Electric and magnetic fields were weighted to particles linearly to be consistent with the charge weighting. Particle velocities and positions were updated with the second order leap-frog algorithm. Methods for loading particles are discussed in the sub-section below.

1. Modified Q1D Boris Push

The conventional Boris pushing algorithm was modified to include the effects of using an axisymmetric coordinate system. Algorithms have been developed for 2D axisymmetric $\hat{r} - \hat{z}$ simulations which simply include a coordinate transformation step for the velocity and position instead of including additional inertial forces.[26] This method fails in the Q1D case because there is not a second coordinate with which to transform the velocity. Therefore we have developed a modified Boris push for the Q1D solver which includes the inertial forces which arise due from the axisymmetric coordinate system. The modified algorithm divided into three steps:

$$\mathbf{v}_1 = \mathbf{v}_0 + \Delta t \left[\frac{q}{2m} \mathbf{E} + \frac{\mathbf{a}_{coord,1}}{2} \right] \tag{10}$$

$$\mathbf{v}_2 = \mathbf{v}_1 + \Delta t \frac{q}{2m} (\mathbf{v}_2 + \mathbf{v}_1) \times \mathbf{B} \tag{11}$$

$$\mathbf{v}_N = \mathbf{v}_2 + \Delta t \left[\frac{q}{2m} \mathbf{E} + \frac{\mathbf{a}_{coord,N}}{2} \right] \tag{12}$$

in which $\mathbf{a}_{coord}$, the acceleration due to inertial effects, is:

$$\mathbf{a}_{coord} = \frac{v_\theta^2}{r_L} \hat{r} - \frac{v_\theta v_r}{r_L} \hat{\theta}. \tag{13}$$

Contributions due coordinate system forces are included in the initial (Equation 10) and final (Equation 12) half time steps of the electric field in the Boris algorithm. The coordinate system forces have dependency on the velocity which results in the initial and final half steps having to be solved implicitly. This implicit solution is significantly simplified by noting the v_θ dependence of r_L and thereby reducing the order of the equations. The magnetic field contributions are incorporated in the intermediate (Equation 11) step using the conventional Boris rotation. This method is referred to as semi-implicit because it is not implicit over the whole algorithm but over the individual steps.

2. *Particle Loading*

Particles velocities can be loaded either randomly or quietly according to a Maxwellian or drifting Maxwellian velocity distribution.[27,28] Maxwellian particle flux sources at boundaries and internal cells has also been incorporated. Drifting Maxwellian flux sources will be incorporated in future simulations.

A method for seeding particles at the boundaries using ghost particles in a ghost cell has also been developed. Particles are loaded in the ghost cell according to a Maxwellian or drifting Maxwellian and then allowed to flux naturally into the domain during the particle push. Particles that do not make it into the domain are deleted and a new set of ghost particles is loaded during the next time step. Initial testing reproduces the flux biased Maxwellian used in the conventional flux source approach.

III. Validation

A. Two Stream Instability

Two opposing streams of particles with a perturbation in their density are unconditionally unstable.[24] Each stream of particles starts with a single velocity and a small perturbation in their density. The density perturbation is equivalent to a perturbation in the electric field. As the counter-flowing streams interact an instability grows which transfers energy from the uniform, directed streams to thermal and electrostatic modes.

To simulate the two stream instability, two streams of like-charged particles are loaded in the domain with non-dimensional velocities equal to $v_x = 1$ and $v_x = -1$. A small sinusoidal perturbation is applied to the density of the particles of each species resulting in a perturbation to the electric field. The domain is one-dimensional in $\hat{x}$ and the boundary conditions are periodic. Input parameters are chosen to match those of Birdsall[24] and a comparison of the results is shown in Figure 4. In this figure the time is non-dimensionalized by the plasma frequency.

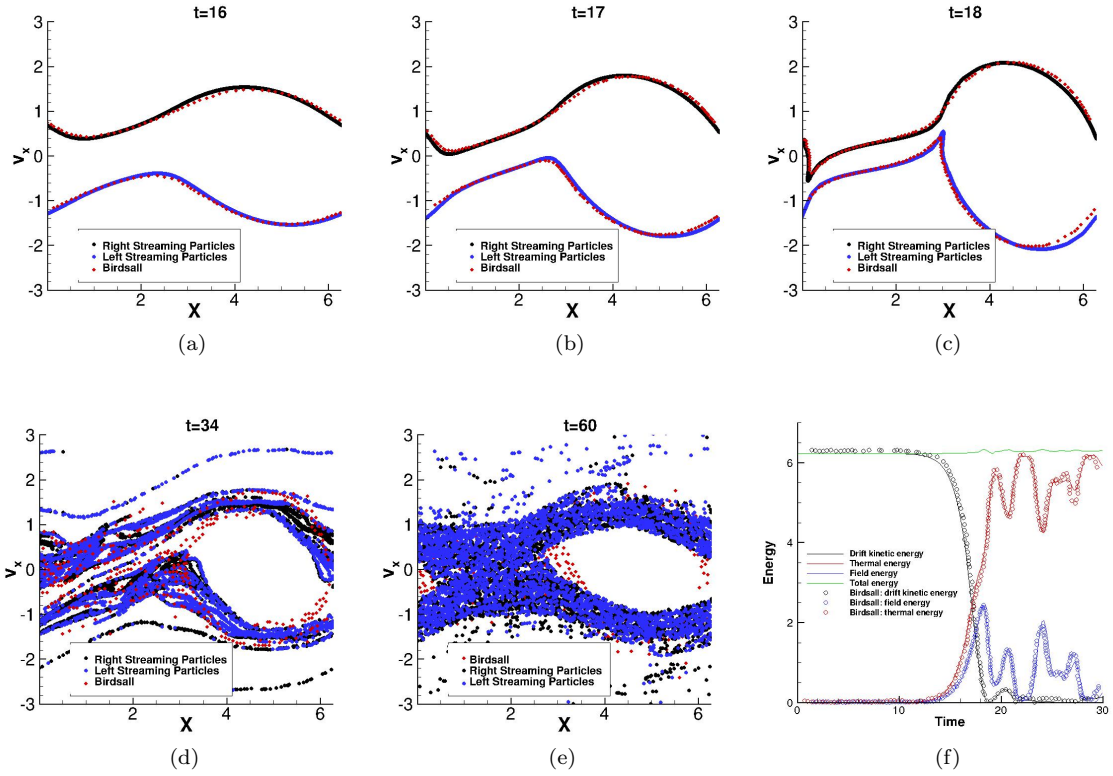

Figure 4: Two stream instability velocity space evolution in time (a-e) and energy time history (f). The time is non-dimensionalized by the plasma frequency. Comparisons with digitized results from Birdsall are shown.[24]

The results from our simulations show good agreement with those from Birdsall. Slight deviations are seen at $t = 60$ which may be due to digitization of the data and slight the differences simulation parameters (i.e. number of particles used). This simulation validates the electrostatic particle mover and interpolation algorithms. The ability of the solver to correctly capture instabilities and instability growth rates is also validated. Oppositely charged two stream instability, warm two stream instability, and beam instability test cases have also been simulated and show good agreement with additional results presented by Birdsall. These cases are not shown here for the sake of brevity.

B. Landau Damping

Damping of electrostatic waves occurs in a plasma even without collisions.[24,28] This phenomenon is called Landau damping and occurs due to the energy exchanged between particles traveling near the phase velocity, $v_{ph} = \omega/k$, of an electrostatic wave and the wave itself. Particles with velocities less than the phase velocity of the wave gain energy from the wave while particles with velocities greater than the wave phase velocity give energy to the wave. In the case of a Maxwellian distribution, there are more particles with velocities less than the wave, resulting in a net transfer of energy from the wave to the particles resulting in damping of the wave.

To further validate the code we performed a simulation of Landau damping. The domain is one dimensional with periodic boundary conditions. A quiet start algorithm is used for loading particle velocities according to a Maxwellian velocity distribution. If particle velocities were loaded randomly, no damping would be seen. The particle density is slightly perturbed to generate an electrostatic wave. Simulation parameters are chosen to match those of Birdsall[24] and Denavit.[28] Using these parameters a damping rate of $\omega_i = -0.15$ is expected. The number of particles selected for our simulation was 10^5 and 10^6 which is different from that of Denavit which used 17711 particles. The reason for this is because the quiet start implemented in our simulations is not as complex as that of Denavit and required additional particles to resolve the Landau damping. The charge and mass (ratio q/m remains the same) of the particles is changed so that all other parameters remain the same. The results of these simulations are shown in Figure 5 which illustrates the damping of the non-dimensionalized electrostatic energy with time.

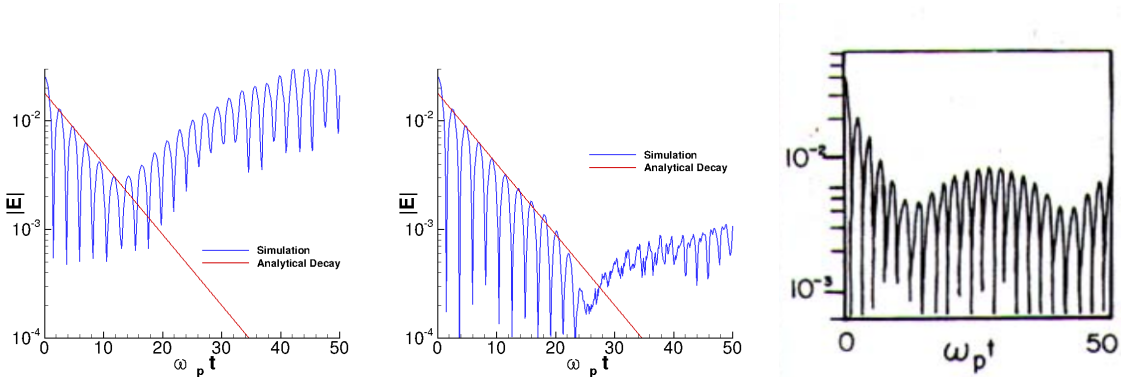

Figure 5: Landua damping simulation comparison with Denavit.[28] (a) Simulation with 10^5 particles,(b) Simulation with 10^6 particles, (c) Results of Denavit with 17711 particles.

The results from Figure 5 show that the code correctly reproduces the analytic damping rate expected for these conditions. The mean electrostatic energy is damped for a finite amount of time after which it oscillates. Ideally, the damping would continue indefinitely, however, the finite number of particles in these simulations limits the amount of damping due to the depletion of particles from the velocity space in which damping occurs. Increasing the number of particles allows the simulation to damp further as illustrated. These simulation results validate the algorithms used to load particles for a quiet start, which is essential to capturing thermal instabilities in PIC simulations.

C. Collector and Source Sheath

Complex phenomena such as the formation of collector and source sheaths are also simulated to validate this solver. The region between a Maxwellian plasma source and a collecting surface is simulated with the one dimensional PIC code and compared with the results of Schwager.[29] The left boundary of the domain is a Maxwellian plasma source which has a net flux of particles into the domain. Particles which reach this boundary from the domain are thermalized according to the source and then reinjected into the domain. No net charge builds up at the injection boundary. The right boundary is an electrically floating collector and net charge accumulation occurs.

For our simulation we selected the case of Schwager in which the electron ion mass ratio (m_{ion}/m_e) is 40, the electrons and ions have the same temperature, and the domain length is 44 Debye lengths (λ_D). The remaining parameters, grid size, and time step are chosen to match those of presented in detail by Schwager.[29]

Figure 6 shows a comparison of the non-dimensionalized potential, ψ, calculated in our simulation results and digitized results of Schwager.[29] In this figure, the potential is non-dimentionalized by the thermal energy, x is the resolved direction, and L is the length of the domain. Our simulation correctly shows the formation of both the source and collector sheath although the magnitude of the potential drop for the source sheath is slightly different. This difference is most likely due to the fact that Schwager used a more advanced code tailored for the simulations of sheaths which includes surface effects and transport evaluation. Some error may also be attributed to the digitization process used to plot the data of Schwager used for comparison.

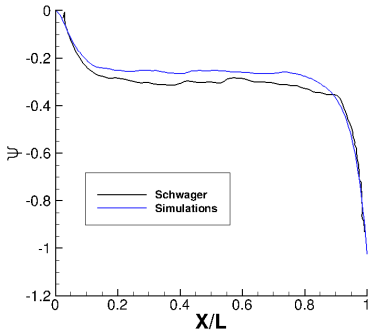

Figure 6: Normalized potential comparison with results of Schwager.[29]

The number densities of electrons and ions in the domain are shown in Figure 7. The results of Schwager are again shown for comparison. The comparisons here are more qualitative due to the difficulty in digitizing the results of Schwager. In both our simulations and those of Schwager it is seen that the ion density is on average higher than the electron density in sheath regions. This is especially true at the collector sheath. The same oscillatory behavior of the density is also seen in both simulations.

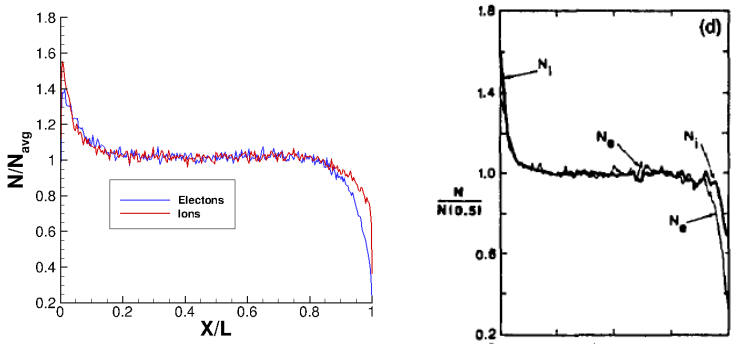

(a) (b)

Figure 7: Normalized density results from our simulations (a) compared to results of Schwager (b).[29]

Sheath simulations validate the code with more complex boundary conditions which include a flux source and collector. These results also illustrate the ability of the code correctly capture complex potential structures.

D. Magnetic Mirror

Magnetic mirrors machines are devices used to confine plasmas. Plasma is generated in a low magnetic field (strong enough for the particles to be magnetized) region which then flows into a converging, high magnetic field region. As the particles move into this region the magnetic field force changes the velocity along the field line into velocity perpendicular to the field line. In some cases the sign of axial velocity can be changed resulting in the particle being reflected away from the high magnetic field region back into the low field region. The high magnetic field region is called a magnetic mirror and particles that meet specific criteria are reflected by these mirrors. Particles which escape are part of what is known as the loss cone. Assuming a constant magnetic moment and kinetic energy of a particle, it is found that the confined particles satisfy the condition shown in Equation 14.[20]

$$\frac{v_\perp^2}{v_\parallel^2 + v_\perp^2} > \frac{B_{min}}{B_{max}} \tag{14}$$

The final test case is that of a magnetic mirror which validates the modifications made to the particle mover for the Q1D code by comparing with magnetic mirror theory. The Q1D algorithm does not assume a constant magnetic moment, but the conditions for this particular simulation satisfy the major assumptions made for a constant magnetic moment. Electric field effects are ignored in order to focus on the Q1D changes made in the magnetic field Lorentz force contributions and the area variation algorithm is not included as this contribution only shows up in the electric field contributions. These simulations represent conditions similar to those in a magnetic nozzle which may include a converging-diverging magnetic field.

For these simulations particles are given velocities according to a Maxwellian distribution and are placed at the center of the domain at which the magnetic field strength is $B_{z,min} = 1\ T$. For simplicity, the charge to mass ratio is equal to one and the charge is that of an electron. The domain length, L, is one meter and the number of grid points is 100. Particles that reach the boundary are removed from the simulation. The magnetic field strength grows as z^2 from the center of the domain. Two cases are presented with the maximum magnetic field strength at the edge of the domain equal to $B_{z,max} = 1.75\ T$ and $B_{z,max} = 4\ T$. The initial and final velocity space of particles is shown in Figure 8 along with the line calculated from Equation 14.

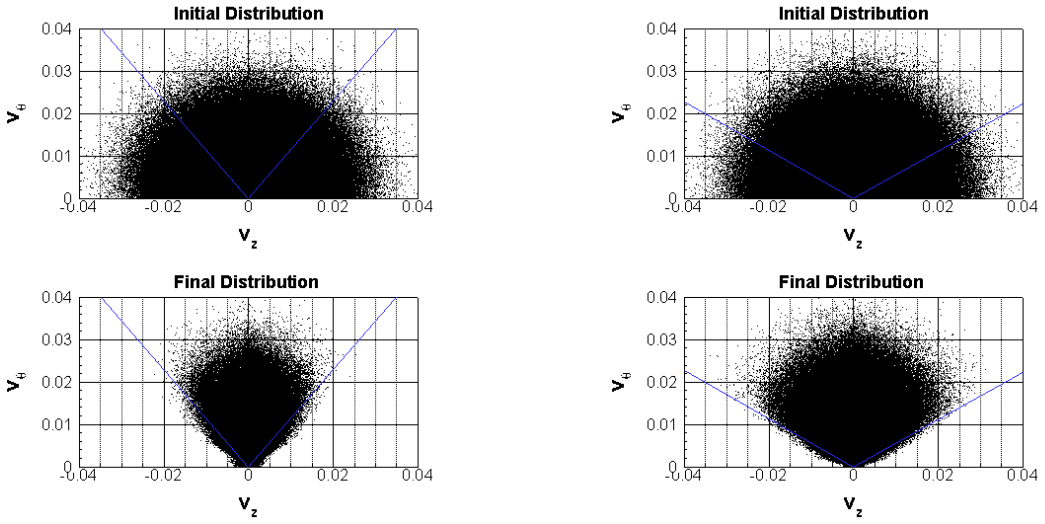

(a) (b)

Figure 8: Intial and final velocity (m/s) distribution in magnetic mirror. (a) $B_{z,max} = 1.75\ T$, (b) $B_{z,max} = 4.0\ T$.

The final velocity space shown in Figure 8 shows the development of the loss cone and how the loss cone shrinks by increasing the magnetic field strength. Reproducing this familiar magnetic mirror behavior illustrates that the Q1D algorithms are producing physically accurate results and can be used to simulate the symmetry axis of the magnetic nozzle.

IV. Conclusions and Future Work

The Q1D PIC code and incorporated algorithms are validated through test cases relevant to magnetic nozzles. We demonstrate the ability of the code to accurately capture instabilities, energy exchange, sheath formation, and magnetic mirror effects which are essential to studying magnetic nozzle physics.

A final test case of a collisionless plasma expansion into a vacuum is planned to further validate code and study the final boundary condition for expansion to a vacuum.[30] Direct comparison with the Cubesat Ambipolar Thruster (CAT) experiments at the Plasmadynamics and Electric Propulsion Lab (PEPL) are planned to further validate the code. The Q1D PIC code will be used in conjunction with this experiment to more deeply understand the physics of magnetic nozzles and optimize the design of the magnetic nozzle.

Acknowledgments

This research is funded by a NASA Office of the Chief Technologist Space Technology Research Fellowship. Thank you to all of my fellow lab mates at PEPL for their insightful discussions concerning this research.

References

[1]C Charles. Plasmas for spacecraft propulsion. *Journal of Physics D: Applied Physics*, 42(16):163001, 2009.

[2]Francis F Chen. Permanent magnet helicon source for ion propulsion. *Plasma Science, IEEE Transactions on*, 36(5):2095–2110, 2008.

[3]R. Winglee, T. Ziemba, L. Giersch, J. Prager, J. Carscadden, and BR Roberson. Simulation and laboratory validation of magnetic nozzle effects for the high power helicon thruster. *Physics of Plasmas*, 14:063501, 2007.

[4]M.D. West, C. Charles, and R.W. Boswell. Testing a helicon double layer thruster immersed in a space-simulation chamber. *Journal of Propulsion and Power*, 24(1):134–141, 2008.

[5]F.N. Gesto, B.D. Blackwell, C. Charles, and R.W. Boswell. Ion detachment in the helicon double-layer thruster exhaust beam. *Journal of Propulsion and Power*, 22(1):24–30, 2006.

[6]K. , T. Lafleur, C. Charles, P. Alexander, RW Boswell, M. Perren, R. Laine, S. Pottinger, V. Lappas, T. Harle, et al. Direct thrust measurement of a permanent magnet helicon double layer thruster. *Applied Physics Letters*, 98(14):141503–141503, 2011.

[7]C Charles, RW Boswell, and MA Lieberman. Xenon ion beam characterization in a helicon double layer thruster. *Applied physics letters*, 89(26):261503–261503, 2006.

[8]F. Ebersohn, S.S. Sharath, D. Staack, J. Shebalin, B. Longmier, and C. Olsen. Magnetic nozzle plasma plume: Review of crucial physical phenomena. AIAA-2012-4274, Atlanta, GA, July 2012.

[9]E. Ahedo and M. Merino. On plasma detachment in propulsive magnetic nozzles. *Physics of Plasmas*, 18:053504, 2011.

[10]J.M. Little, A.S. Rubin, and E.Y. Choueiri. Similarity parameter evolution within a magnetic nozzle with applications to laboratory plasmas. IEPC-2011-229, Wiesbaden, Germany, September 2011.

[11]K. Kuriki and O. Okada. Experimental study of a plasma flow in a magnetic nozzle. *Physics of Fluids*, 13:2262, 1970.

[12]M. Inutake, K. Hattori, A. Ando, F. Hori, T. Sugirnura, K. Fukushi, T. Ochiai, M. as aya Yamamoto, T. Yagai, A. Imasaki, et al. Supersonic plasma flow in a magnetic nozzle. Proc. of the 26th IEPC, 1999.

[13]B.W. Longmier, E.A. Bering, M.D. Carter, L.D. Cassady, W.J. Chancery, F.R.C. Díaz, T.W. Glover, N. Hershkowitz, A.V. Ilin, G.E. McCaskill, et al. Ambipolar ion acceleration in an expanding magnetic nozzle. *Plasma Sources Science and Technology*, 20:015007, 2011.

[14]Justin M Little and Edgar Y Choueiri. Thrust and efficiency model for electron-driven magnetic nozzles. *Physics of Plasmas (1994-present)*, 20(10):103501, 2013.

[15]A.V. Arefiev and B.N. Breizman. Ambipolar acceleration of ions in a magnetic nozzle. *Physics of Plasmas*, 15:042109, 2008.

[16]J.C. Sercel. Simple model of plasma acceleration in a magnetic nozzle. In *AIAA, DGLR, and JSASS, 21st International Electric Propulsion Conference*, volume 1, 1990.

[17]HG Kosmahl. Three-dimensional plasma acceleration through axissymmetric divergine magnetic fields based on dipole moment approximation. Technical report, National Aeronautics and Space Administration,Lewis Research Center, Cleveland, OH, 1967.

[18]F.R. Chang-Diaz. The vasimr rocket. *Scientific American*, 283(5):90–97, 2000.

[19]J.D. Jackson. *Classical electrodynamics*. Wiley, 1999.

[20]F.F. Chen. *Introduction to Plasma Physics and Controlled Fusion*, volume 1. Plenum Press, New York, 1984.

[21]Albert Meige, Rod W Boswell, Christine Charles, and Miles M Turner. One-dimensional particle-in-cell simulation of a current-free double layer in an expanding plasma. *Physics of plasmas*, 12:052317, 2005.

[22]T Lafleur and RW Boswell. Particle-in-cell simulations of ambipolar and nonambipolar diffusion in magnetized plasmas. *Physics of Plasmas*, 19:053505, 2012.

[23]Adam B Sefkow and Samuel A Cohen. Particle-in-cell modeling of magnetized argon plasma flow through small mechanical apertures. *Physics of Plasmas*, 16:053501, 2009.

[24]Charles K Birdsall and A Bruce Langdon. *Plasma physics via computer simulation*. CRC Press, 2004.

[25]John P Verboncoeur. Particle simulation of plasmas: review and advances. *Plasma Physics and Controlled Fusion*, 47(5A):A231, 2005.

[26]JP Boris. Relativistic plasma simulation-optimization of a hybrid code. In *Proc. Fourth Conf. Num. Sim. Plasmas, Naval Res. Lab, Wash. DC*, pages 3–67, 1970.

[27]KL Cartwright, JP Verboncoeur, and CK Birdsall. Loading and injection of maxwellian distributions in particle simulations. *Journal of Computational Physics*, 162(2):483–513, 2000.

[28]J Denavit and JM Walsh. Nonrandom initializations of particle codes. *Comments Plasma Phys. Control. Fusion*, 6:209–223, 1981.

[29]Lou Ann Schwager and Charles K Birdsall. Collector and source sheaths of a finite ion temperature plasma. *Physics of Fluids B: Plasma Physics (1989-1993)*, 2(5):1057–1068, 1990.

[30]J Denavit. Collisionless plasma expansion into a vacuum. *Physics of Fluids (1958-1988)*, 22(7):1384–1392, 1979.